Journal of Zhejiang University-SCIENCE A (Applied Physics & Engineering) in press
www.jzus.zju.edu.cn; www.springer.com/journal/11582
E-mail: jzus_a@zju.edu.cn

Research Article

https://doi.org/10.1631/jzus.A2400216

Hydraulic conductivity of sand influenced by temperature and porosity in centrifugal tests

Jianjian HE, Xihao JIANG, Yubing WANG✉

Center for Hypergravity Experiment and Interdisciplinary Research, College of Civil Engineering and Architecture, Zhejiang University, Hangzhou 310058, China

Abstract: This study focused on the hydraulic conductivity of sand in centrifuge modeling. A self-designed temperature-controlled falling-head permeameter apparatus was used, and a series of falling-head seepage tests were performed on sand samples with various porosities at different temperatures and centrifugal accelerations. The objectives were to qualitatively and quantitatively investigate the effects of temperature, porosity, and centrifugal acceleration on the hydraulic conductivity of sand and to study the applicability of the Kozeny-Carman equation for the centrifugal environment. Test results showed that in a similar temperature range and under the same porosity, the hydraulic conductivity of the sand is linearly correlated with centrifugal acceleration; when subjected to the same centrifugal acceleration and in a similar temperature range, the hydraulic conductivity of the sand exhibits an almost linear increase in relation to its porosity function ($s^3/(1-s)^2$); the functional relationships between the hydraulic conductivity of the sand and temperature (T), centrifugal acceleration level (n), and porosity (s) were established using two pathways; and when the centrifugal acceleration is less than 50g, the Kozeny-Carman equation is effectively accurate in predicting the hydraulic conductivity of sand; however, when the centrifugal acceleration exceeds 50g, it is important to consider a significant error.

Key words: Hydraulic conductivity of sand; Temperature; Porosity; Centrifugal acceleration; Kozeny-Carman equation

1 Introduction

The physical model test is a fundamental research approach in geotechnical engineering, and centrifuge modeling is a significant experimental technique within the physical model test. Due to its capacity to accurately replicate the stress state of a prototype, ensuring consistency in the deformation and failure mechanisms between the model and the prototype (Chen et al., 2011), centrifuge modeling is commonly favored as an experimental technique (Ng, 2014). Many centrifuge model tests are related to seepage, such as those of rainfall-induced landslides (Ling and Ling, 2012; Chen et al., 2019), dam breaches (Mei et al., 2022; Zhang et al., 2023), seepage behavior of dams (Wang et al., 2013; Ye et al., 2021), and contaminant migration (Zeng et al., 2022; Zheng et al., 2022). Therefore, in-depth research on the seepage characteristics of soils in a centrifugal environment is of great significance for solving various seepage-related geotechnical engineering problems.

Permeability is a crucial engineering property of soil (Joshaghani and Ghasemi-Fare, 2021). The hydraulic conductivity is a specific characterization of the permeability of soil, and is an essential parameter for studying the seepage field and assessing the deformation and stability of geotechnical structures when subjected to water-related factors like rainfall and changes in water level (Su et al., 2014). Therefore, many researchers have conducted in-depth studies on the hydraulic conductivity of soil in a 1g environment (Cho et al., 1999; Wang et al., 2010; Ye et al., 2013; Ng and Coo, 2015). There are many factors that influence the hydraulic conductivity of soil, such as the porosity (Su et al., 2014; Li et al., 2024), particle

✉ Yubing WANG, wangyubing@zju.edu.cn
Jianjian HE, https://orcid.org/0000-0002-8583-1641
Yubing WANG, https://orcid.org/0000-0002-2398-6007

Received Apr. 24, 2024; Revision accepted June 14, 2024; Crosschecked

© Zhejiang University Press 2024

Unedited

shape (Wang et al., 2017; Li et al., 2024), particle size distribution (Su et al., 2014; Wang et al., 2017), temperature (Ye et al., 2013; Joshaghani and Ghasemi-Fare, 2021), and impact load (Li et al., 2024). While there has been little research on the factors that affect the hydraulic conductivity of soil in centrifuge modeling, a significant amount of research has been dedicated to validating the scaling law of hydraulic conductivity in theory (Schofield, 1980; Tan and Scott, 1985; Taylor, 1987; Butterfield, 2000; Thusyanthan et al., 2003). Some scholars have used experimental methods to verify the scaling law of hydraulic conductivity (Singh and Gupta, 2000; Wang et al., 2011; Van Tonder and Jacobsz, 2017). That is, by testing the hydraulic conductivity of soil in a centrifugal environment (k_{cen}) and comparing it with the hydraulic conductivity of a 1g scale (k_p), the scaling ratio (k_{cen}/k_p) of hydraulic conductivity can be obtained. However, these researchers have found that the k_{cen}/k_p obtained from experiments is not equal to the theoretical scaling law. The reasons for this phenomenon may involve insufficient length of the centrifuge arm, non-uniformity of the centrifugal acceleration field, soil consolidation, and other factors (Sharma and Samarasekera, 2007; Wang et al., 2011). However, we believe that another possible reason for this phenomenon is the lack of temperature control on the model during the experimental process, as the hydraulic conductivity is significantly influenced by temperature. In the above studies, the measurement of the hydraulic conductivity of soil was not rigorous enough and so the influence of temperature on hydraulic conductivity was neglected. Therefore, studies of the effect of temperature on hydraulic conductivity in centrifuge modeling are needed and are of great significance for improving the fundamental theory of centrifuge modeling.

In addition, the coupled temperature-hydraulic-mechanical (THM) behavior of soil has become one of the main focuses and challenges in geotechnical engineering in recent years, and is relevant for applications such as underground energy engineering (Sailer et al., 2021), natural gas hydrate exploitation (Ye et al., 2022), and nuclear waste disposal (Zhao et al., 2016). Centrifuge modeling has also been extensively used to investigate these challenges (Ng et al., 2021; Wang et al., 2022). The hydraulic conductivity of soil is one of the crucial parameters for accurately describing the coupled THM behavior of soil. For example, Xiong (2018) used COMSOL software to analyze the thermo-hydro coupling in saturated sand, building upon prior centrifuge test results, and found that in a centrifugal environment, hydraulic conductivity has a substantial influence on the thermo-hydro coupling effect in saturated soil. Nevertheless, researchers have not adequately addressed the influence of temperature on hydraulic conductivity in a centrifugal environment. This deficiency may have had a negative impact on the precise replication of soil THM coupling behavior by centrifuge modeling. Therefore, accurately revealing and characterizing the influence of temperature on the hydraulic conductivity of soil in a centrifugal environment is crucial for using centrifuge modeling to accurately depict the coupled THM behavior of soil and is also of significant importance for addressing multifield coupling problems in geotechnical engineering.

The experimental measurement of soil hydraulic conductivity exhibits remarkable accuracy and extensive practicality. Nevertheless, the process of experimentally determining soil hydraulic conductivity can be laborious and time-consuming. Consequently, numerous scholars have proposed theoretical prediction equations for soil hydraulic conductivity based on the soil's inherent properties and a large amount of experimental data (Aubertin et al., 1996; Chapuis, 2004; Li et al., 2023; Zhong et al., 2023; Fan and Rowe, 2024). The Kozeny-Carman hydraulic conductivity prediction equation (hereinafter referred to as the Kozeny-Carman equation; Carman, 1939; Nomura et al., 2018) is widely used. The applicability of the hydraulic conductivity prediction equations mentioned above has been extensively confirmed in a 1g environment. Nevertheless, few studies have considered the suitability of these hydraulic conductivity prediction equations in a centrifugal environment. Also, no equation for predicting soil hydraulic conductivity has been proposed that is acceptable for a centrifugal environment.

Sand is a common material found in many geotechnical structures, including dams (Wen et al., 2015; Eisma et al., 2020; Li et al., 2021), embankments (Zhao et al., 2021; Ikbarieh et al., 2023; Qin et al., 2024), tunnel strata (Yang et al., 2021;

Unedited

Cheng et al., 2023; Khalajzadeh et al., 2023), and foundation pits (Li et al., 2018; Sun et al., 2019; Gao et al., 2023). Therefore, investigating the hydraulic conductivity of sand under the influence of multiple factors is of significant practical importance for the safe operation and maintenance of geotechnical structures. However, previous studies (Singh et al., 2000; Wang et al., 2011; Van Tonder and Jacobsz, 2017) focused mainly on clay, with little research on sand. Therefore, to address the research gaps mentioned above, in this study we used a self-designed temperature-controlled falling-head permeameter apparatus to conduct centrifuge modeling. A series of falling-head seepage tests were performed on sand samples with various porosities at different temperatures and centrifugal accelerations. The main aims of this study were: (1) to investigate the effects of temperature, porosity, and centrifugal acceleration on the hydraulic conductivity of sand; (2) to establish quantitative relationships between hydraulic conductivity, temperature, porosity, and centrifugal acceleration; and (3) to verify the applicability of the Kozeny-Carman equation for a centrifugal environment.

2 Experimental setup

2.1 Test setup

To conduct seepage tests at different temperatures in a centrifugal environment, a self-designed temperature-controlled falling-head permeameter apparatus was used for the centrifuge modeling. A schematic view of the apparatus is shown in Fig. 1. This paper simply provides a brief introduction to the apparatus. The apparatus has a temperature-controlled falling-head permeameter, several transducer modules (such as a temperature transducer module, a pore water pressure transducer module, and a flow meter module) and their data acquisition system, an electric ball valve module and its remote-control system, an upstream water supply reservoir, a downstream water collection reservoir, and a constant-temperature water bath circulation system for the centrifuge. The temperature-controlled falling-head permeameter is the core component of the apparatus. It is used to regulate the temperature of soil samples and fluids and conduct falling-head tests. The rest of the apparatus is linked to the temperature-controlled falling-head permeameter as follows:

(1) The pore water pressure transducer module consists of several pore water pressure transducers that are linked to pore water pressure monitoring channels (not marked in Fig. 1) located on the base pedestal of the temperature-controlled falling-head permeameter. The pore water pressure monitoring holes are located on the soil column cylinder and are numbered Hole 1, Hole 2, Hole 3, and Hole 4 (Fig. 1). The soil column cylinder is separated into two sections: the 160-mm-tall soil sample area is located below, and the 145-mm-tall fluid area is located above. The center of Hole 4 is positioned 30 mm above the bottom of the soil sample; the distance between the centers of Hole 3 and Hole 4, as well as between the centers of Hole 3 and Hole 2, is 50 mm; the distance between the centers of Hole 1 and Hole 2 is 35 mm. A total of five pore water pressure transducers were used in this study. To accurately measure the water level in the fluid area, two pore water pressure transducers, labeled $P_{1\text{-}1}$ and $P_{1\text{-}2}$ respectively, were placed in Hole 1. One pore water pressure transducer was installed at each of Hole 2, Hole 3, and Hole 4, labeled P_2, P_3, and P_4, respectively. The accuracy of all the pore water pressure transducers was 0.2%.

(2) The temperature transducer module has several temperature transducers positioned on the top cap of the temperature-controlled falling-head permeameter. These transducers provide immediate monitoring of the temperature of the fluid area and the water bath chamber. Three temperature transducers were used in this study, labeled T_1, T_2, and T_3, respectively. T_1 was positioned at the center of the water bath chamber to monitor the temperature of the water bath chamber. T_2 was located at the edge of the fluid area, near the wall of the soil column cylinder, to monitor the temperature of the fluid at the edge of the fluid area. T_3 was positioned in the middle of the fluid area to monitor the temperature of the center of the fluid area. The measurement range for T_1, T_2, and T_3 was from -50 to 50 ℃.

(3) The flow meter module consists of several flow meters linked to the flow monitoring channel (not marked in Fig. 1) placed on the base pedestal of the temperature-controlled falling-head permeameter.

Unedited

(4) The electric ball valve module is made up of multiple electric ball valves, some of which are coupled in series with flow meters so that tests can be started and stopped remotely. These electric ball valves are also connected to a downstream water collection reservoir, which is used to collect seepage fluid. In addition, an electric ball valve is connected in series with the upstream water supply reservoir, which provides seepage fluid to the fluid area.

(5) To regulate the temperature of soil samples and fluids, the temperature-controlled falling-head permeameter's top cap and base pedestal are equipped with water bath channels (not marked in Fig. 1) that are connected to the constant-temperature water bath circulation system.

(6) The centrifuge's transducer data acquisition system measures and gathers information from the transducers. Moreover, a PC can be used to remotely operate the electric ball valves.

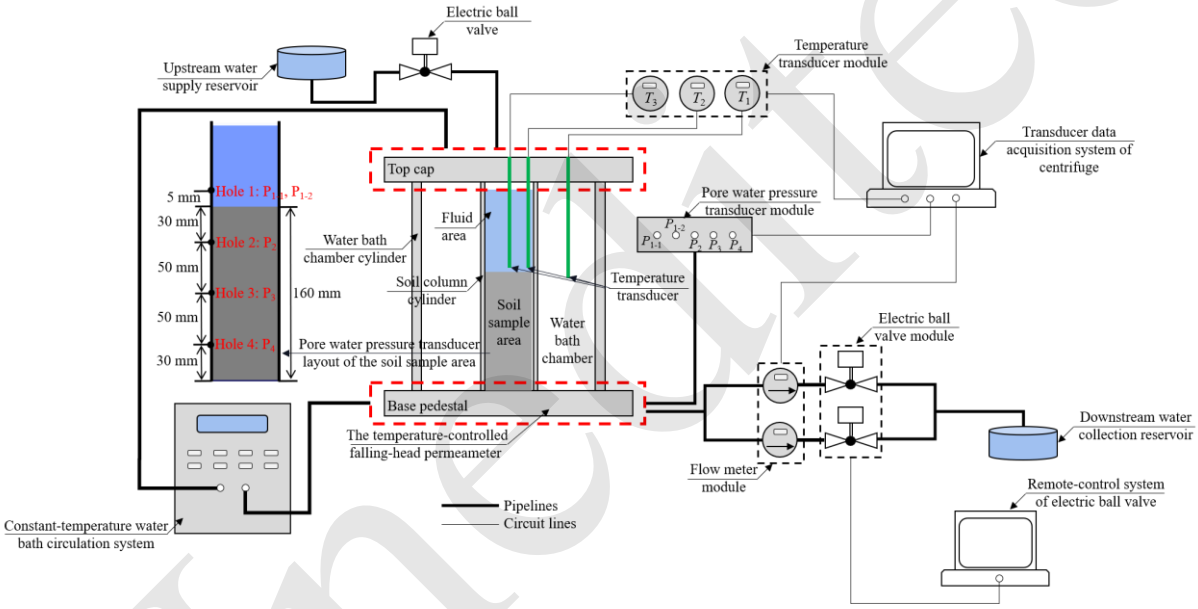

Fig. 1 A schematic view of the temperature-controlled falling-head permeameter apparatus

2.2 Test materials and test plan

The test soil, with particles ranging from 0.075 to 0.25 mm in size, was separated from ISO-standard sand from China. Fig. 2 shows the particle size distribution of the test soil. The specific gravity of the test soil was 2.631. The test soil had maximum and minimum void ratios of 0.956 and 0.589, respectively. The fluid used in this study was airless water.

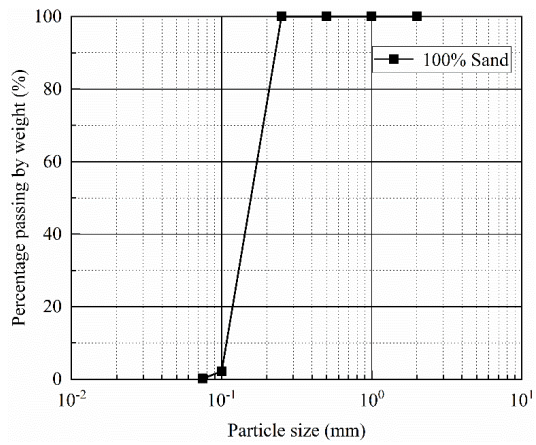

Fig. 2 Particle size distribution curve of test soil

This study mainly investigated the effects of

Unedited

temperature, centrifugal acceleration, and porosity on the hydraulic conductivity of sand. Accordingly, a total of 36 temperature-controlled falling-head tests were carried out in a centrifugal environment (Table 1). Table 1 shows the test temperatures for the soil samples. The temperatures outside the parentheses represent the actual test temperatures, while the temperatures inside the parentheses indicate the desired set temperatures for the constant-temperature water bath circulation system (Fig. 1) to achieve the corresponding test temperatures of the soil samples. Table 1 shows that: (1) For the soil sample with a porosity of 0.381, the temperature settings for the constant-temperature water bath circulation system differed significantly from the temperature settings for the soil samples with the other two porosities. The reason for this discrepancy is that we conducted that test in the summer (early July), while we conducted the other two tests in the spring (early April). In summer, the temperature control efficiency of the constant-temperature water bath circulation system is lower than in spring, especially for low-temperature control. For instance, if we set the constant-temperature water bath circulation system to 10.5 ℃ for the soil sample with a porosity of 0.381, we could control the soil sample test temperatures to 13.2 ℃, 16.0 ℃, and 18.9 ℃ at 15g, 30g, and 50g, respectively. This was mainly because in summer, the greater the centrifugal acceleration, the faster the rotational speed of the centrifuge, resulting in increased heat generation. Consequently, the low-temperature control effectiveness of the water bath circulation system diminished. Therefore, although the constant-temperature water bath circulation system was set to 10.5 ℃, it could maintain the soil sample test temperatures at only 13.2 ℃, 16.0 ℃, and 18.9 ℃ at 15g, 30g, and 50g, respectively. The soil samples with porosities of 0.420 and 0.458 did not exhibit this phenomenon. (2) During high-temperature control, the greater the centrifugal acceleration, the greater the convection, and thus, the higher the temperature control efficiency of the constant-temperature water bath circulation system. For example, if we set the constant-temperature water bath circulation system to 42.0 ℃ for the soil sample with a porosity of 0.420, we could adjust the soil sample test temperatures to 42.2 ℃, 41.2 ℃, and 41.2 ℃ for 15g, 30g, and 50g, respectively. We observed the same phenomenon in the soil sample with a porosity of 0.458. The relative density of the sand used in the experiment was 0.93, 0.63, and 0.30, respectively, corresponding to void ratios of 0.615, 0.725, and 0.846 and corresponding porosities of 0.381, 0.420, and 0.458, respectively.

Table 1 Test plan

Centrifugal acceleration (g)	Porosity: 0.381	Porosity: 0.420	Porosity: 0.458
	Test temperature (℃)	Test temperature (℃)	Test temperature (℃)
15	13.2 (10.5), 23.2 (22.5), 32.7 (33.5), 42.2 (45.0)	12.7 (9.0), 21.6 (19.0), 32.2 (31.0), 42.2 (42.0)	13.0 (10.0), 22.5 (20.0), 32.4 (31.0), 43.5 (42.5)
30	16.0 (10.5), 26.4 (26.0), 36.4 (37.5), 45.3 (48.5)	12.7 (9.0), 21.3 (19.0), 31.8 (31.0), 41.2 (42.0)	13.6 (10.0), 22.2 (20.0), 32.2 (31.0), 42.4 (42.5)
50	18.9 (10.5), 29.2 (29.0), 39.0 (40.5), 49.2 (53.0)	12.8 (9.0), 21.5 (19.0), 32.0 (31.0), 41.2 (42.0)	13.8 (10.0), 22.3 (20.0), 32.2 (31.0), 42.5(42.5)

Note: The temperatures outside the parentheses represent the actual test temperatures, while those inside the parentheses indicate the desired sett temperatures for the constant-temperature water bath circulation system (Fig. 1) to achieve the corresponding test temperatures for the soil samples.

2.3 Test preparation in a 1g environment

Several test preparations were completed in a 1g environment, including the following steps:

(1) Preparation of a soil sample. The sand was oven-dried and subsequently used to make the samples using the dry tamping method (Zhu et al., 2021). Each soil sample had a diameter of 60 mm and a height of 160 mm. It was compacted into eight layers, each 20 mm thick.

(2) Saturation of the soil sample. Each soil sample was saturated in two stages: first with carbon dioxide for 3 h and then with airless water for 12 h.

(3) Installation of the model. After saturation, the temperature-controlled falling-head permeameter and other equipment were placed in the model box. Then the model box was installed in the centrifuge (Fig. 3).

(4) Regulation of soil sample temperature.

Unedited

Following the installation of the model, the water bath circulation system was turned on to regulate the fluid and soil sample temperatures at the desired levels.

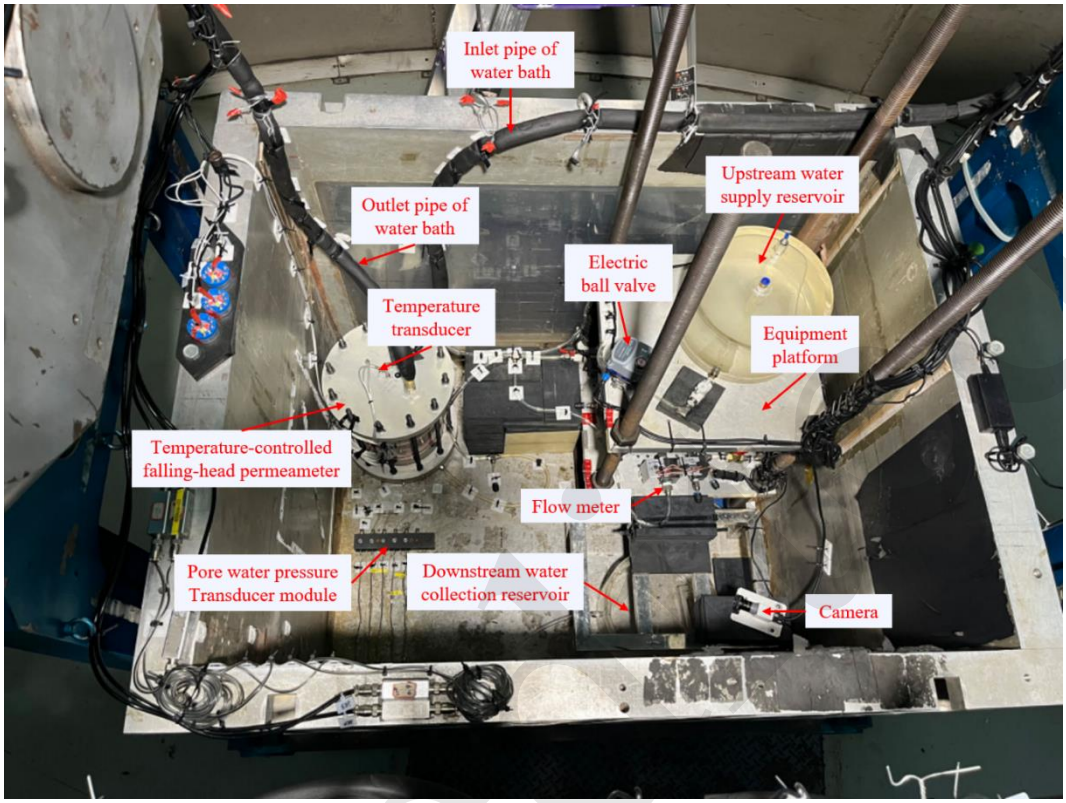

Fig. 3 Apparatus after installation in the ZJU400 centrifuge

2.4 Test procedure in a centrifugal environment

Experiments were carried out using the ZJU-400 centrifuge at Zhejiang University, which has a spinning radius of 4.5 m, a maximum centrifugal acceleration of 150g, a maximum capacity of 400 g t, and a basket volume of 1.5×1.2×1.5 m. Once the temperature control procedure in a 1g environment was completed, the centrifuge was started. The test procedure for a single test was as follows:

(1) Step I: Fill the fluid area. The current test is marked as Test N. After Test N is completed, the downstream electric ball valve is shut, while the electric ball valve upstream of the upstream water supply reservoir is opened. Then, fluid is injected into the fluid area, and once full, the electric ball valve of the upstream water supply reservoir is closed.

(2) Step II: Adjust the temperature. After completing Step I, the water bath temperature is adjusted to the predetermined temperature for the subsequent test, which is labeled as Test N+1.

(3) Step III: Adjust the centrifuge acceleration. After completing Step II, adjust the centrifuge acceleration to the target value of Test N+1.

(4) Step IV: Test the apparatus's sealing. After completing Step III, monitor the values of all pore water pressure transducers. If the values remain stable, it indicates good sealing of the apparatus. Conversely, if the values change, it suggests water leakage in the apparatus. In this study, based on the pore water pressure transducers' values, we inferred that the apparatus maintained good sealing under all experimental conditions.

(5) Step V: Conduct the test. After completing Step IV, carefully observe the readings of the three temperature transducers, and after reaching the target temperature for Test N+1, choose the suitable flow meter, activate the relevant electric ball valve to conduct the test, and then shut the ball valve after the test is finished.

Note that in this study, after a single test was completed, the soil sample was not refilled. This is because using a single sample can reduce the differences in soil properties caused by refilling, making the test results more comparable. The properties of soil samples are significantly influenced by the preparation process. In our tests, the soil samples needed to undergo four temperature ranges (around 13 ℃, 23 ℃, 33 ℃, and 43 ℃). We would have needed four samples if we were to perform refills after each temperature range. Ensuring that these four samples had very similar soil properties would have been a substantial challenge. From this perspective, using the same sample throughout the entire testing process offered greater control over the soil properties compared to refilling. This significantly enhanced the comparability of the test results obtained.

3 Results and Discussion

3.1 Temperature regulation

Fig. 4 shows the changes in water bath temperature (T_1) and fluid temperatures (T_2, T_3) over time before and during seepage for a sand sample with a porosity of 0.458 in a 50g environment when the experimental temperature was 13.8 ℃ and 42.5 ℃, respectively, which correspond to low and high temperature test conditions. Fig. 4 shows that, before seepage, the water bath circulation system consistently adjusted the fluid temperature and maintained it constant after reaching the desired temperature. Fig. 4 also indicates that although the fluid's temperature progressively rose during the seepage process, it did not exceed a 0.5 ℃ change during the entire seepage test, thereby meeting the test requirement that the apparatus can precisely control the temperature of sand samples and fluids. The other tests gave the same results and so are not shown in this paper.

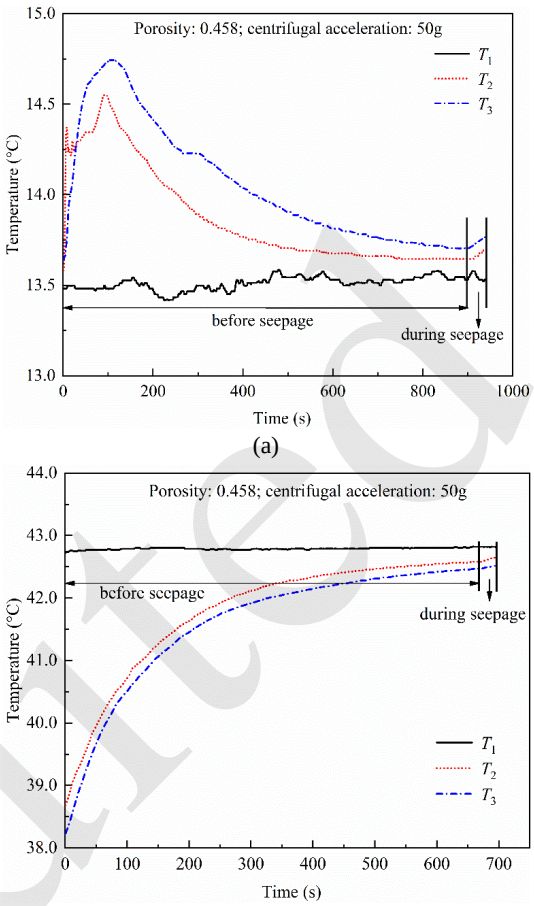

Fig. 4 Variation of water bath temperature (T_1) and fluid temperature (T_2, T_3) with time: (a) the experimental temperature was 13.8 ℃; (b) the experimental temperature was 42.5 ℃

3.2 Seepage water head process line

When a falling-head seepage test is carried out, the seepage stability of the soil sample is directly reflected by the change in the seepage water head over time, which is called the seepage water head process line. Fig. 5 illustrates the variations in the seepage water head (h_1) over time of sand with various porosities under different temperatures and centrifugal accelerations. The values of seepage water head (h_1) were calculated from the pore water pressure transducers $P_{1\text{-}1}$ or $P_{1\text{-}2}$ (for calculation details, see Section 3.3.1). Fig. 5 shows that the seepage water heads of the three sand samples gradually decreased with time, and the rate of decline of each seepage water head process line was stable, indicating that the seepage of the samples under each test condition was stable and

Unedited

the results of each test were reliable. With the same porosity, the rate of decline of the seepage water head is related to factors such as centrifugal acceleration and temperature: the greater the centrifugal acceleration, the higher the temperature, and the faster the rate of decline. Although the seepage water head process lines of "15g, 13 ℃" and "15g, 12.7 ℃" in Figs. 5a and 5b differed somewhat from the others, this was due to the initial water head difference in these two tests being relatively low. This initial condition caused the rate of decrease in water head at the beginning of the test to be slower than that in the other tests.

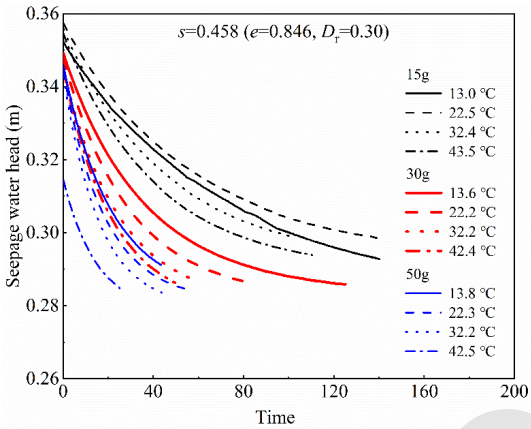

(a)

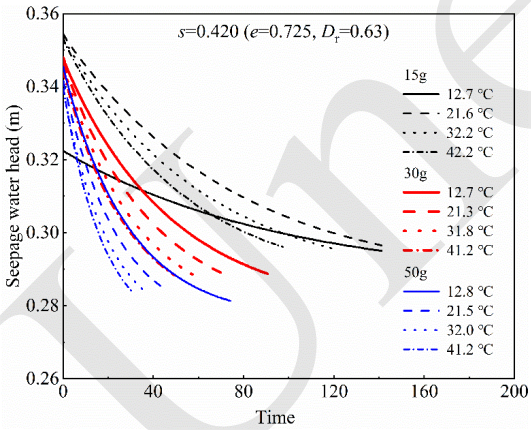

(b)

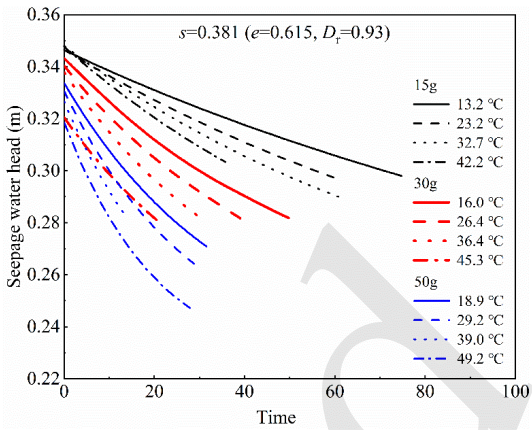

(c)

Fig. 5 The change in seepage water head of sand samples with time: (a) *s*=0.458; (b) *s*=0.420; (c) *s*=0.381

3.3 Hydraulic conductivity

3.3.1 Calculation of hydraulic conductivity

The main focus of this study was on the hydraulic conductivity of the whole sand sample; we did not look into the layered hydraulic conductivity. Thus, the calculation of hydraulic conductivity was limited to the sand sample located between Hole 2 and Hole 4. The following equation was used to calculate each sand sample's hydraulic conductivity:

$$k_{\mathrm{T}} = \frac{QL_0}{AHt} \tag{1}$$

where k_{T} is the hydraulic conductivity at T ℃, in cm/s; Q is the flow rate in t seconds, in cm^3; L_0 is the distance between the centers of two pore water pressure monitoring holes, in cm; A is the cross-sectional area of the soil sample, in cm^2; H is the total head difference between the centers of two pore water pressure monitoring holes, obtained by the relationship between the water head and the pore water pressure, in cm; and t is the test duration, in seconds. When using Eq. (1), the seepage should satisfy Darcy's Law. To check the validity of Darcy's law, we used the Reynolds number (Re): $Re = \rho vd/\mu$, where ρ is fluid density, v is seepage velocity, d is soil characteristic microscopic length (such as the effective particle size d_{10}), and μ is the fluid dynamic viscosity coefficient (Singh and Gupta, 2000). Darcy's law is applicable to seepage

Unedited

through soils provided that the *Re* remains below 1. In the present study, the *Re* was calculated on the basis of d_{10} (which was 0.108 mm). The maximum value of *Re* of all tests was 0.90 (i.e., $Re < 1$), which indicates the validity of Darcy's law in this study.

To calculate the total head difference, *H*, it is necessary to convert the pore water pressure into the water head. The specific conversion process is as follows: When the soil column is positioned eccentrically, the calculation diagram of the total head at any point in the soil sample is as shown in Fig. 6. Given the non-uniformity of the centrifugal field and the eccentric positioning of the soil column, the centrifugal acceleration value *N*' at any given height of h_0 from plane *E* (which serves as the datum plane) in the soil sample is

$$N' = \frac{n\mathrm{g}}{R}\sqrt{L^2 + \left(R_0 - h_0\right)^2} \tag{2}$$

Considering the small eccentricity in this experiment, we assumed that the centrifugal acceleration direction of the permeameter's central axis remained perpendicular to the bottom of the model box. Where $R_0=R-d_1-d_2$; *R* is the maximum effective rotation radius of the centrifuge; *L* is eccentricity distance; d_1 is the model box base thickness; d_2 is the distance between Plane E and the top surface of the model box base; and *n* is the centrifugal acceleration level, from Eq. (2), we can obtain the total head height of h_0 when the total pore water pressure is

$$P = \int_0^{h_0} \rho \frac{n\mathrm{g}}{R}\sqrt{L^2 + \left(R_0 - h\right)^2}\,\mathrm{d}h \tag{3}$$

Using Eq. (3), we used Matlab to solve the value of the total head corresponding to pore water pressure.

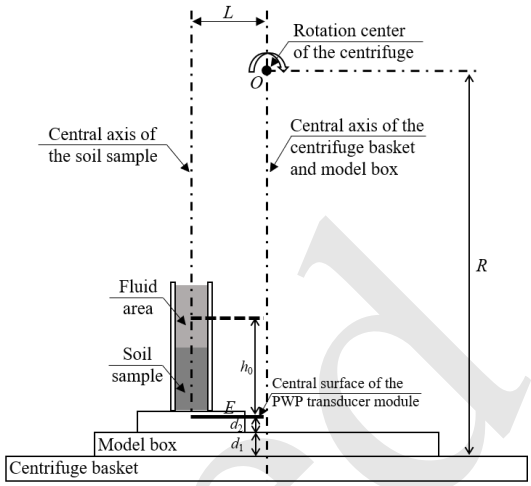

Fig. 6 Calculation diagram of the total head at any point in the sand sample

3.3.2 Changes in hydraulic conductivity with centrifugal acceleration under the same porosity

In this study we adopted the viewpoint that the hydraulic conductivity of soil changes with centrifugal acceleration in centrifuge modeling (Singh and Gupta, 2000; Garnier et al., 2007; Wang et al., 2011). Fig. 7 illustrates how the hydraulic conductivity of sand with different porosities changed with centrifugal acceleration in a similar temperature range. The above-mentioned hydraulic conductivity is the hydraulic conductivity at real temperature, not at 20 ℃, and the temperature-controlled falling-head tests were conducted at about 13 ℃, 23 ℃, 33 ℃, and 43 ℃. The real temperature is the average temperature of the entire seepage process. Fig. 7 shows that in a similar seepage temperature range, no matter how dense the sand (the porosities of 0.381, 0.420, and 0.458 correspond to loose sand, medium dense sand, and dense sand, respectively, in this study), the hydraulic conductivity of the sand was linearly correlated with centrifugal acceleration. In other words, the higher the centrifugal acceleration, the greater the hydraulic conductivity of sand, which is similar to the phenomenon that clay's hydraulic conductivity increases with increasing centrifugal acceleration (Wang et al., 2011).

Unedited

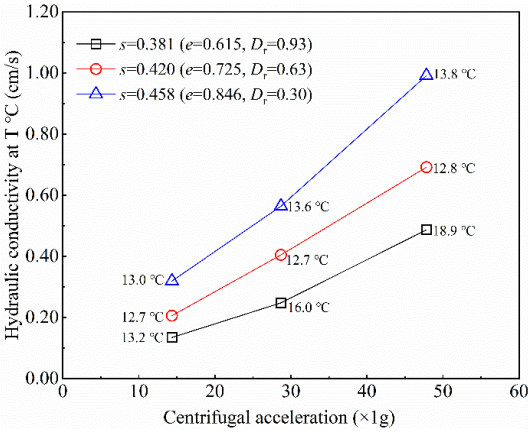

(a)

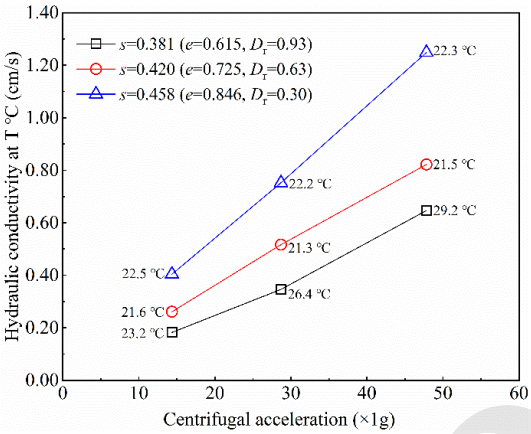

(b)

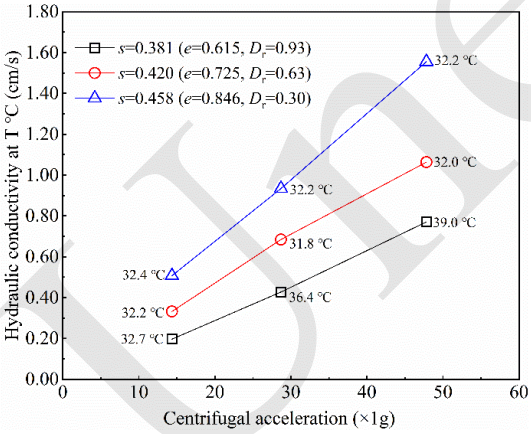

(c)

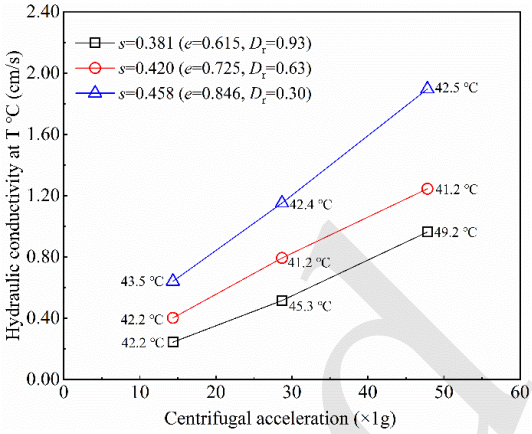

(d)

Fig. 7 The hydraulic conductivity of sand samples with different porosity varies with centrifugal acceleration in a similar temperature range: (a) around 13 ℃; (b) around 23 ℃; (c) around 33 ℃; (d) around 43 ℃

3.3.3 Changes in hydraulic conductivity with porosity under the same centrifugal acceleration

The Kozeny-Carman equation can effectively predict the hydraulic conductivity of soil in a 1g environment, and one of its forms is as follows (Flint and Selker, 2003; Wang et al., 2011):

$$k = \frac{d_{\mathrm{m}}^2}{180} \frac{s^3}{(1-s)^2} \frac{\rho g}{\mu} \tag{4}$$

where d_{m} is the characteristic particle size of the soil and g is the acceleration due to gravity. Therefore, to establish the relationship between the hydraulic conductivity of sand and its porosity in a centrifugal environment, we introduce a porosity function based on the Kozeny-Carman equation. Specifically, we refer to $s^3/(1\text{-}s)^2$ in Eq. (4) as the porosity function.

We plotted the relationship between hydraulic conductivity and the porosity function ($s^3/(1\text{-}s)^2$) of sand in similar temperature ranges (around 13, 23, 33, and 43 ℃) under three centrifugal accelerations (15g, 30g, and 50g), as shown in Fig. 8. From Fig. 8, it can be observed that: (1) Under the same centrifugal acceleration and in a similar temperature range, the porosity of sand increased, and its hydraulic conductivity also increased, consistent with results from experiments conducted in a 1g environment (Su et al., 2014). This is because as po-

Unedited

rosity increases, the volume of pores within a unit volume of soil also increases. This leads to a larger cross-sectional area for fluid flow through the soil under the same hydraulic head pressure, resulting in an increase in hydraulic conductivity (Su et al., 2014). (2) Under the same centrifugal acceleration and in a similar temperature range, the hydraulic conductivity of sand showed a nearly linear growth in relation to its porosity function ($s^3/(1-s)^2$). This trend aligns with the findings of studies carried out in a 1g environment by Su et al. (2014).

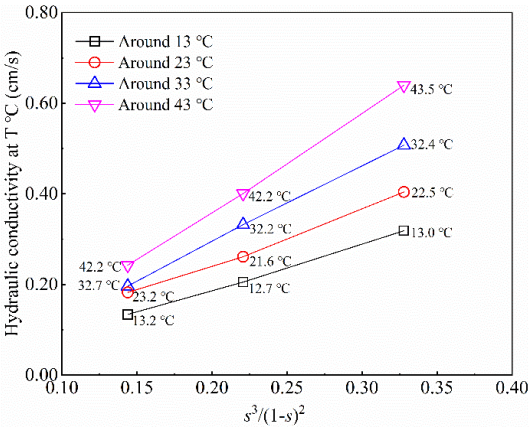

(a)

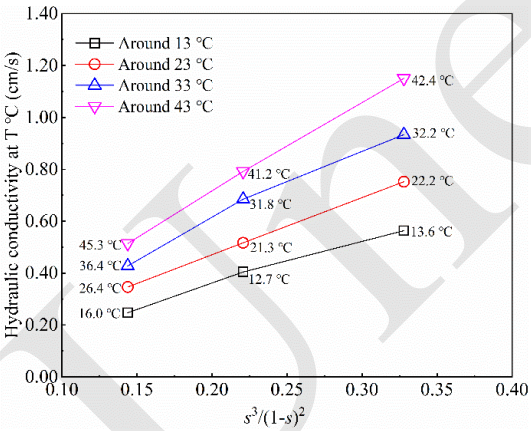

(b)

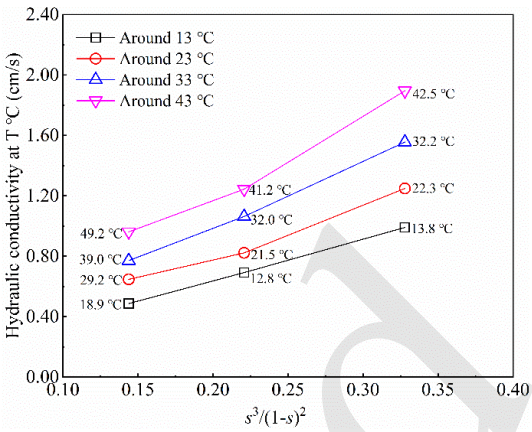

(c)

Fig. 8 The relationship between the hydraulic conductivity and porosity function ($s^3/(1-s)^2$) of sand in similar temperature ranges under different centrifugal accelerations: (a) 15g; (b) 30g; (c) 50g

3.4 Quantitative analysis of the influence of multiple factors on the hydraulic conductivity of sand

Under the interaction of the centrifugal environment (*n*g), temperature (*T*), and soil pores (*s*), the hydraulic conductivity of sand may differ from that measured in a 1g environment. Hydraulic conductivity has a significant impact on issues like soil consolidation and the liquefaction of sand in a centrifugal environment. Therefore, quantitative analysis of the influence of multiple factors, such as centrifugal acceleration, temperature, and porosity, on the hydraulic conductivity of sand in centrifuge modeling becomes extremely important. In this study, the hydraulic conductivity (*k*) was a ternary function, denoted as $k=k\ (n,\ T,\ s)$. Therefore, it is necessary to first establish the relationship between the hydraulic conductivity and temperature, porosity, denoted as $k=k\ (T,\ s)$, or the relationship between the hydraulic conductivity and centrifugal acceleration, porosity, denoted as $k=k\ (n,\ s)$. Then, the function $k=k\ (n,\ T,\ s)$ can be derived. In the following section, we will introduce these two methods separately.

3.4.1 Establishing $k\ (n,\ T,\ s)$ based on $k\ (T,\ s)$

Firstly, the hydraulic conductivities of sand samples at the real temperature in the 15g environment were normalized to hydraulic conductivities at 15, 25, 35, and 45 ℃. The

Unedited

normalized process involves changing the hydraulic conductivity measured at the real temperature to the hydraulic conductivity at a particular temperature. To illustrate, the process of normalizing the hydraulic conductivity at the real temperature of 13.2 ℃ ($k_{13.2}$) to the hydraulic conductivity at 15 ℃ (k_{15}) was determined using the equation $k_{15}=k_{13.2}\times(\mu_{13.2}/\mu_{15})$, where $\mu_{13.2}$ and μ_{15} represent the dynamic viscosity coefficients of the fluid at 13.2 ℃ and 15 ℃, respectively. Subsequently, the relationship between the normalized hydraulic conductivity and the porosity function $s^3/(1\text{-}s)^2$ was plotted, followed by linear regression analysis (Fig. 9). Fig. 9 shows that there was a linear positive correlation between the normalized hydraulic conductivity and the porosity function $s^3/(1\text{-}s)^2$. This means that the normalized hydraulic conductivity and the porosity function $s^3/(1\text{-}s)^2$ have the following relationship:

$$k_{\mathrm{T}}=a\frac{s^3}{(1-s)^2}+b \tag{5}$$

where parameters a and b are obtained by fitting.

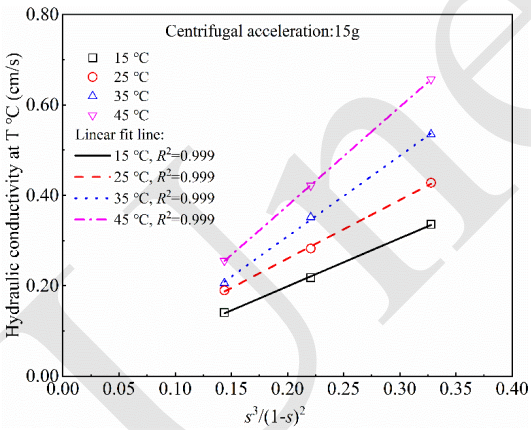

Fig. 9 The relationship between the normalized hydraulic conductivity and the porosity function $s^3/(1\text{-}s)^2$ in the 15g environment

The parameter a of 15g and temperature T have a strong linear relationship, which satisfies the following equation:

$$a=cT+b \tag{6-1}$$

where parameters c and d are obtained by linear fitting. Specifically, in this study,

$$a=0.03844T+0.4293, R^2=0.983 \tag{6-2}$$

Substituting Eq. (6-1) into Eq. (5), the quantitative predictive equation for the hydraulic conductivity of sand, considering the influence of multiple factors in centrifuge modeling, can be obtained:

$$k(T,s)=cT\frac{s^3}{(1-s)^2}+d\frac{s^3}{(1-s)^2}+b \tag{7}$$

Eq. (7) is derived based on the normalized hydraulic conductivity in a 15g environment. To verify the applicability of Eq. (7), it was used to fit the hydraulic conductivity at actual temperatures under different centrifugal accelerations (Fig. 10). Fig. 10 shows that under various centrifugal accelerations, Eq. (7) provides good fitting results for the hydraulic conductivities at real temperatures of sand samples at different porosities.

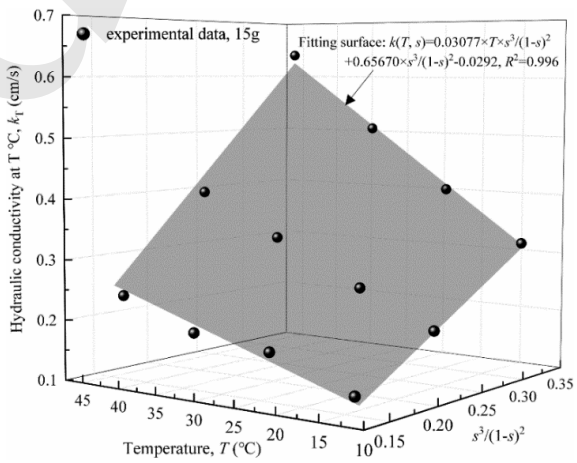

(a)

Unedited

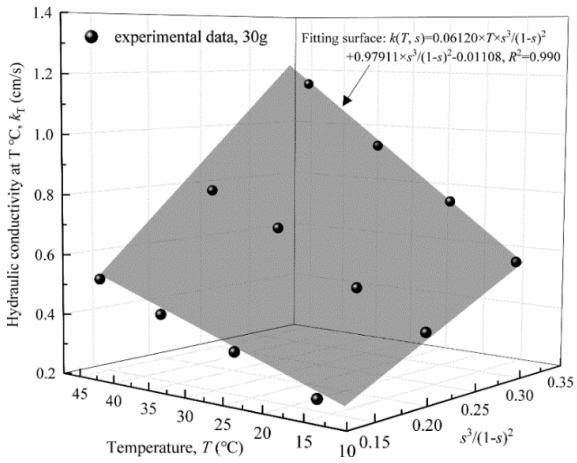

(b)

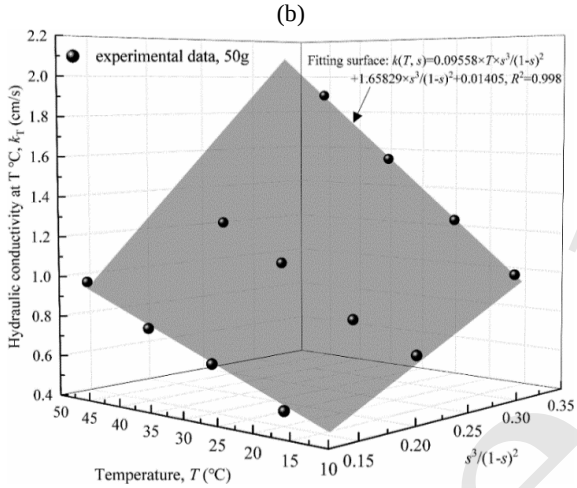

(c)

Fig. 10 Using Eq. (7) to fit the hydraulic conductivity at real temperatures under different centrifugal accelerations: (a) 15g; (b) 30g; (c) 50g

The parameter c and the centrifugal acceleration level n satisfy

$$c=fn+j \tag{8-1}$$

Specifically, in this study,

$$c=0.00193n+0.00410,\ R^2=0.998 \tag{8-2}$$

The parameter d and the centrifugal acceleration n level satisfy

$$d=on+u \tag{9-1}$$

Specifically, in this study,

$$d=0.03023n+0.18255,\ R^2=0.986 \tag{9-2}$$

Substituting Eq. (8-2) and Eq. (9-2) into Eq. (7), we obtain

$$k(n,T,s)=0.00193nT\frac{s^3}{(1-s)^2}+0.00410T\frac{s^3}{(1-s)^2}+0.03023n\frac{s^3}{(1-s)^2}+0.18255\frac{s^3}{(1-s)^2}-0.0292 \tag{10}$$

Hence, we have established a quantitative relationship between the hydraulic conductivity and factors such as temperature, porosity, and centrifugal acceleration level in centrifuge modeling by first establishing the relationship between the hydraulic conductivity and temperature and porosity.

3.4.2 Establishing k (n, T, s) based on k (n, s)

Firstly, the hydraulic conductivities of sand samples around 23 ℃ were normalized to 25 ℃. In accordance with Garnier et al. (2007), we support that there was a linear positive correlation between the normalized hydraulic conductivity and the centrifugal acceleration level:

$$k_T=a_1 n \tag{11}$$

Subsequently, the relationship between the normalized hydraulic conductivity and centrifugal acceleration level under the same porosity was plotted, followed by linear regression analysis (Fig. 11).

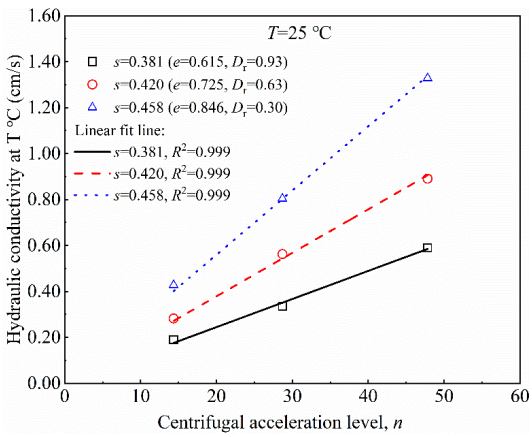

Fig. 11 The relationship between the normalized hy-

Unedited

draulic conductivity at 25 ℃ and the centrifugal acceleration level

There is a linear relationship between parameter a_1 of 25 ℃ and the porosity function $s^3/(1\text{-}s)^2$, which satisfies the following equation:

$$a_1 = b_1 \frac{s^3}{(1-s)^2} \tag{12-1}$$

where parameter b_1 is obtained by linear fitting. After substituting Eq. (12-1) into Eq. (11), the hydraulic conductivity and the centrifugal acceleration level still satisfy the linear positive correlation. Specifically, in this study,

$$a_1 = 0.08539 \frac{s^3}{(1-s)^2}, R^2 = 0.999 \tag{12-2}$$

Substituting Eq. (12-1) into Eq. (11), the quantitative predictive equation for the hydraulic conductivity of sand, considering the influence of multiple factors in centrifuge modeling, can be obtained:

$$k(n,s) = b_1 n \frac{s^3}{(1-s)^2} \tag{13}$$

Eq. (13) is derived based on the normalized hydraulic conductivity. To verify the applicability of Eq. (13), it was used to fit the hydraulic conductivity at real temperatures (Fig. 12). Fig. 12 shows that Eq. (13) provides good fitting results for the hydraulic conductivities at actual temperatures of sand samples at different porosities and different centrifugal acceleration levels.

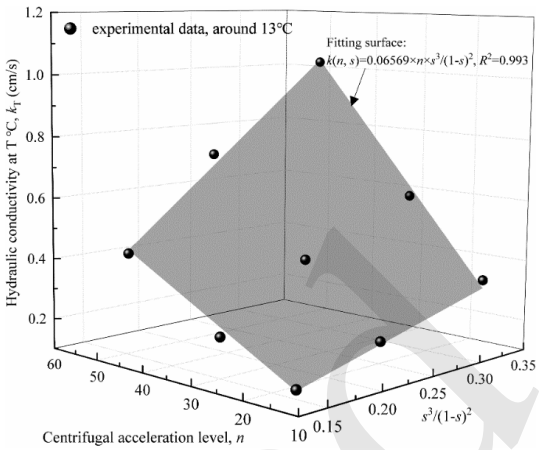

(a)

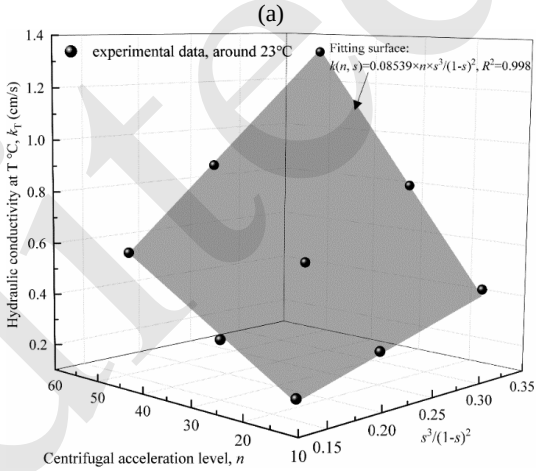

(b)

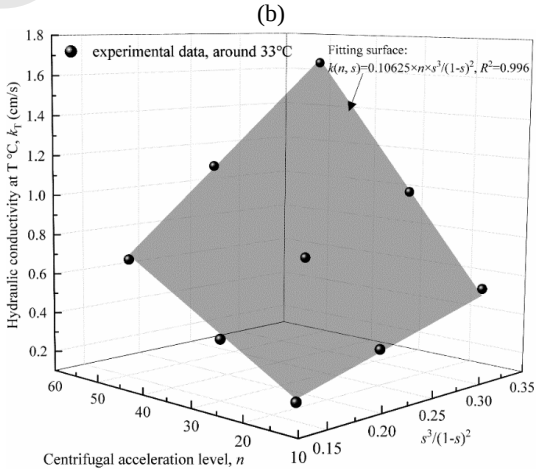

(c)

Unedited

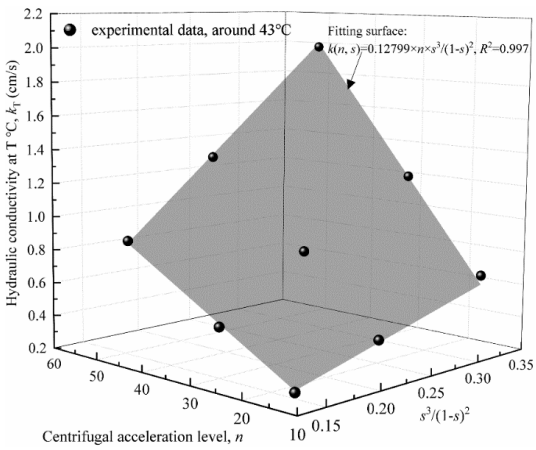

(d)

Fig. 12 Using Eq. (13) to fit the hydraulic conductivity at real temperatures: (a) around 13 ℃; (b) around 23 ℃; (c) around 33 ℃; (d) around 43 ℃

The parameter b_1 and the temperature T satisfy

$$b_1=d_1T+j_1 \tag{14-1}$$

Specifically, in this study,

$$b_1=0.00208T+0.03400,\ R^2=0.999 \tag{14-2}$$

Substituting Eq. (14-2) into Eq. (13), we obtain

$$k(n,T,s)=0.00208nT\frac{s^3}{(1-s)^2}+0.03400n\frac{s^3}{(1-s)^2} \tag{15}$$

Thus, we have established a quantitative relationship between the hydraulic conductivity and factors such as temperature, porosity, and the centrifugal acceleration level, by first establishing the relationship between the hydraulic conductivity and centrifugal acceleration level and porosity. The quantitative relationships between the hydraulic conductivity and temperature, porosity, and centrifugal acceleration level derived by the two methods, namely Eqs. (10) and (15), show some discrepancies. We will discuss these differences later.

3.5 Applicability of Kozeny-Carman equation to centrifuge modeling

In Section 3.4, based on the porosity function from the Kozeny-Carman equation, we established the relationships between the hydraulic conductivity and temperature, porosity, and centrifugal acceleration level. From this, we also inferred that the Kozeny-Carman equation may be used to predict the hydraulic conductivity of sand in a centrifugal environment. Therefore, in this section, we validate the applicability of the Kozeny-Carman equation to centrifuge modeling. The relevant parameters in the Kozeny-Carman equation (Eq. (4)) were determined as follows:

According to the particle size distribution curve of the soil samples in this study (Fig. 2), the gradation equation for the soil with diameters ranging from 0.10 mm to 0.25 mm is as follows:

$$y=245.80426\lg x+247.98890 \tag{16}$$

where y represents a percentage, and the unit of x is millimeters. The d_m typically uses either d_{10} or d_{20}, etc. The relationship between the water's dynamic viscosity (Chen et al., 2019) and temperature within the range of 10 ℃ to 50 ℃ satisfies the following:

$$\mu=\frac{1}{26.42042T+471.29372} \tag{17}$$

In this study, we used d_{10} or d_{20}, which, according to the gradation equation (Eq. (16)), equals 0.108 mm or 0.118 mm, respectively. Substituting d_m and Eq. (17) into Eq. (4) and considering the influence of the centrifugal environment (that is, multiplied by n), the Kozeny-Carman equation is obtained as follows:

When d_m is d_{10}

$$k(n,T,s)=0.00168nT\frac{s^3}{(1-s)^2}+0.02993n\frac{s^3}{(1-s)^2} \tag{18-1}$$

When d_m is d_{20}

$$k(n,T,s)=0.00200nT\frac{s^3}{(1-s)^2}+0.03573n\frac{s^3}{(1-s)^2}$$

Unedited

(18-2)

Eq. (18-2) is essentially similar in form to Eq. (15). Thus, we believe that the Kozeny-Carman equation can accurately estimate the hydraulic conductivity of sand in centrifuge modeling under the various conditions of this study's experiments. However, its applicability to a wider range of test conditions requires further study, and as discussed in Section 3.6.

3.6 Discussion

Table 2 presents the hydraulic conductivity prediction equation of sand in centrifuge modeling that was obtained in this study. First, we discuss the reasons for the differences between Eqs. (10) and (15) as well as Eq. (18-2). Comparing Eq. (10) with Eq. (15), it is evident that Eq. (15) is missing three terms, specifically $0.00410\cdot T\,s^3/(1\text{-}s)^2$, $0.18255\,s^3/(1\text{-}s)^2$, and -0.0292. The occurrence of -0.0292 is due to the parameter b in Eq. (5), and when porosity s tends to 0, b tends to 0. Fig. 10 shows also that the corresponding values of b for 15g, 30g, and 50g are -0.0292, 0.01108, and 0.01405, respectively. When compared with the actual hydraulic conductivity, this term can be considered negligible. There are still two missing terms, specifically $0.00410\cdot T\,s^3/(1\text{-}s)^2$ and $0.18255\,s^3/(1\text{-}s)^2$. The discrepancy may be attributed to our assumption in obtaining Eq. (15) that the hydraulic conductivity of soil is directly proportional to the centrifugal acceleration level, as stated in Eq. (11). Some studies (Singh and Gupta, 2000; Wang et al., 2011) have shown that the hydraulic conductivity of soil in centrifuge modeling exhibits a direct correlation with n^{χ}, where χ is close to 1, which may be due to the soil's re-compression in a centrifugal environment. Hence, while applying Eq. (11) for fitting, there may be a certain degree of error. Meanwhile, considering that the coefficients in Eq. (18-2) were obtained from parameters under a 1g scaling without considering the influence of the centrifugal environment, overall, Eq. (10) is closer to the actual situation in centrifuge modeling than Eq. (15) and Eq. (18-2). Eq. (10) more comprehensively considers the influence of factors such as the centrifugal environment, and thus is more suitable for predicting the hydraulic conductivity of sand in centrifugal tests.

Table 2 Summary of prediction equations

Equation number	Specific expression
Eq. (10)	$k(n,T,s)=0.00193nT\frac{s^3}{(1-s)^2}+0.00410T\frac{s^3}{(1-s)^2}$ $+0.03023n\frac{s^3}{(1-s)^2}+0.18255\frac{s^3}{(1-s)^2}-0.0292$
Eq. (15)	$k(n,T,s)=0.00208nT\frac{s^3}{(1-s)^2}+0.03400n\frac{s^3}{(1-s)^2}$
Eq. (18-2)	$k(n,T,s)=0.00200nT\frac{s^3}{(1-s)^2}+0.03573n\frac{s^3}{(1-s)^2}$

As previously stated, in the specific experimental settings of this study (with a temperature range of 12 to 49 ℃ and a maximum centrifugal acceleration of 50g), Eqs. (15) and (18-2), similar to Eq. (10), would exhibit accurate prediction capabilities. However, for larger centrifugal accelerations and higher temperatures, the predictive performance of Eqs. (15) and (18-2) is unclear. Therefore, we compared the hydraulic conductivities calculated by Eqs. (10), (15), and (18-2) under higher temperatures (up to 60 ℃, Ko et al., 2013) and greater centrifugal accelerations (up to 350g, Hou and Wang, 2023). Fig. 13 shows the hydraulic conductivities calculated by Eqs. (10), (15), and (18-2) at different temperatures plotted against the centrifugal acceleration level. Since the phenomena under the two other porosities are consistent with those at a porosity of 0.420, only the figure for a porosity of 0.420 is provided.

Unedited

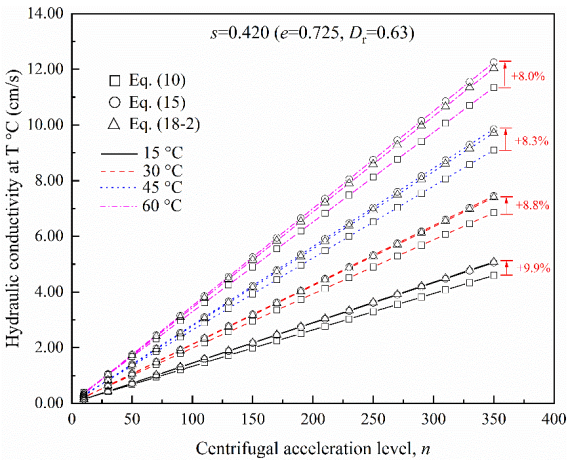

Fig. 13 The variation of hydraulic conductivities calculated by Eqs. (10), (15), and (18-2) with centrifugal acceleration level

Fig. 13 shows that at the same temperature, when the centrifugal acceleration is less than 50g, the hydraulic conductivities calculated by the above three equations are relatively close. This is because when the centrifugal acceleration is less than 50g, the soil compression caused by the centrifugal environment is minimal. Even though Eqs. (15) and (18-2) do not fully consider the influence of the centrifugal environment on the hydraulic conductivity of sand, the results obtained from them are very close to those obtained from Eq. (10), which is consistent with the conclusions of this study. Therefore, when the centrifugal acceleration is less than 50g, all three equations above can be used. When the centrifugal acceleration exceeds 50g, the hydraulic conductivities calculated by Eqs. (15) and (18-2) start to significantly exceed those calculated by Eq. (10), and as the centrifugal acceleration increases, this phenomenon becomes more pronounced. For example, at 15, 30, 45, and 60 ℃, the hydraulic conductivities at 350g calculated by Eq. (15) are respectively 9.9%, 8.8%, 8.3%, and 8.0% higher than those calculated by Eq. (10). This is because when the centrifugal acceleration exceeds 50g, the soil compression caused by the centrifugal environment becomes increasingly significant. As Eqs. (15) and (18-2) do not fully consider the influence of the centrifugal environment on hydraulic conductivity, significant discrepancies start to appear compared to the results obtained by Eq. (10). Therefore, when the centrifugal acceleration exceeds 50g, it is recommended to prioritize the use of Eq. (10). Of course, Eqs. (15) and (18-2) can still be used, but the associated errors must be considered.

4 Conclusions

In this study we used a temperature-controlled falling-head permeameter apparatus to conduct centrifuge modeling. A series of falling-head seepage tests were performed on sand samples with various porosities at different temperatures and centrifugal accelerations. Based on the results, the following conclusions were made:

(1) The centrifuge test results show that in a similar temperature range, no matter how dense the sand, the hydraulic conductivity of the sand is linearly correlated with centrifugal acceleration; when subjected to the same centrifugal acceleration and in a similar temperature range, the hydraulic conductivity of the sand exhibits an almost linear increase in relation to its porosity function ($s^3/(1-s)^2$).

(2) Two pathways were used to obtain functional equations for the hydraulic conductivity of the sand in centrifuge modeling, considering the influencing factors of temperature (T), centrifugal acceleration level (n), and porosity (s). The functional equation obtained by pathway I is as follows:

$$k(n,T,s)=0.00193nT\frac{s^3}{(1-s)^2}+0.00410T\frac{s^3}{(1-s)^2}+0.03023n\frac{s^3}{(1-s)^2}+0.18255\frac{s^3}{(1-s)^2}-0.0292 \tag{10}$$

and the functional equation obtained by pathway II is as follows:

$$k(n,T,s)=0.00208nT\frac{s^3}{(1-s)^2}+0.03400n\frac{s^3}{(1-s)^2} \tag{15}$$

(3) We assessed the applicability of the specific expression of the Kozeny-Carman

Unedited

equation in this study (Eq. (18-2)), as well as Eqs. (15) and (10). When the centrifugal acceleration is less than 50g, the three equations are highly reliable for forecasting the hydraulic conductivity of sand. When the centrifugal acceleration exceeds 50g, it is advisable to give priority to the use of Eq. (10). Eqs. (15) and (18-2) can still be used, but their associated errors must be considered.

Acknowledgments

We gratefully acknowledge financial support for this work from the Basic Science Center Program for Multiphase Media Evolution in Hypergravity of the National Natural Science Foundation of China (Grant No. 51988101).

Author contributions

Conceptualization contributed by Jianjian He, Yubing Wang; methodology by Jianjian He, Xihao Jiang; data collection by Jianjian He, Xihao Jiang; formal analysis and investigation by Jianjian He, Yubing Wang; funding acquisition by Yubing Wang; supervision by Yubing Wang. The first draft of the manuscript was written by Jianjian He, and all authors commented on previous versions. All authors read and approved the final manuscript.

Data availability

The datasets generated during and/or analysed during the current study are available from the corresponding author on reasonable request.

Conflict of interest

Jianjian HE, Xihao JIANG, and Yubing WANG declare that they have no conflict of interest.

References

Aubertin M, Bussiere B, Chapuis RP, 1996. Hydraulic conductivity of homogenized tailings from hard rock mines. *Canadian Geotechnical Journal*, 33(3): 470-482. https://cdnsciencepub.com/doi/10.1139/t96-068

Butterfield R, 2000. Scale-modeling of fluid flow in geotechnical centrifuges. *Soils and Foundations*, 40(6): 39-45. https://doi.org/10.3208/sandf.40.6_39

Carman PC, 1939. Permeability of saturated sands, soils and clays. *Journal of Agricultural Science*, 29(2): 262-273. https://doi.org/10.1017/S0021859600051789

Chapuis RP, 2004. Predicting the saturated hydraulic conductivity of sand and gravel using effective diameter and void ratio. *Canadian Geotechnical Journal*, 41(5): 787-795. https://cdnsciencepub.com/doi/10.1139/t04-022.

Chen MH, Pan HL, Qi MZ, 2019. Principles of chemical engineering, 3rd Edition. East China University of Science and Technology Press, Shanghai, China, p.278-279 (in Chinese).

Chen YL, Irfan M, Uchimura T, et al., 2019. Development of elastic wave velocity threshold for rainfall-induced landslide prediction and early warning. *Landslides*, 16(5): 955-968. https://doi.org/10.1007/s10346-019-01138-2

Chen YM, Han C, Ling DS, et al., 2011. Development of geotechnical centrifuge ZJU400 and performance assessment of its shaking table system. *Chinese Journal of Geotechnical Engineering*, 33(12): 1887-1894 (in Chinese).

Cheng C, Jia PJ, Ni PP, et al., 2023. Upper bound analysis of longitudinally inclined EPB shield tunnel face stability in dense sand strata. *Transportation Geotechnics*, 41: 101031. https://doi.org/10.1016/j.trgeo.2023.101031

Cho WJ, Lee JO, Chun KS, 1999. The temperature effects on hydraulic conductivity of compacted bentonite. *Applied Clay Science*, 14(1-3): 47-58. https://doi.org/10.1016/S0169-1317(98)00047-7

Eisma JA, Merwade VM, 2020. Investigating the environmental response to water harvesting structures: a field study in Tanzania. *Hydrology and Earth System Sciences*, 24(4): 1891-1906. https://doi.org/10.5194/hess-24-1891-2020

Fan JY, Rowe RK, 2024. An empirical equation predicting the saturated hydraulic conductivity of tailings. *Canadian Geotechnical Journal*, in press. https://doi.org/10.1139/cgj-2023-0339

Flint LE, Selker JS, 2023. Use of porosity to estimate hydraulic properties of volcanic tuffs. *Advances in Water Resources*, 26(5): 561-571. https://doi.org/10.1016/S0309-1708(02)00182-3

Gao XH, Tian WP, Li JC, et al., 2023. Research on the stress and deformation characteristics of circular foundation pit during excavation in sand soil. *Advances in Materials Science and Engineering*, 3008695. https://doi.org/10.1155/2023/3008695

Garnier J, Gaudin C, Springman SM, et al., 2007. Catalogue of scaling laws and similitude questions in geotechnical centrifuge modeling. *International Journal of Physical Modelling in Geotechnics*, 7(3): 1-23. https://doi.org/10.1680/ijpmg.2007.070301

Hou YJ, Wang X, 2023. Construction and operation of geotechnical centrifuge laboratories. *Chinese Journal of Geotechnical Engineering*, 45(11): 2396-2402 (in Chinese). https://doi.org/10.11779/CJGE20210909

Ikbarieh A, Izadifar M, Abu-Farsakh MY, et al., 2023. A parametric study of embankment supported by geosynthetic reinforced load transfer platform and timber piles tip on sand. *Transportation Geotechnics*, 38: 100901.

Unedited

https://doi.org/10.1016/j.trgeo.2022.100901

Joshaghani M, Ghasemi-Fare O, 2021. Exploring the effects of temperature on intrinsic permeability and void ratio alteration through temperature-controlled experiments. *Engineering Geology*, 293: 106299. https://doi.org/10.1016/j.enggeo.2021.106299

Khalajzadeh AK, Choobbasti AJ, Kutenaei SS, 2023. Dynamic behaviour of a circular tunnel in the sand: A numerical verification of a centrifuge program. *Tunnelling and Underground Space Technology*, 138: 105152. https://doi.org/10.1016/j.tust.2023.105152

Ko HJ, Ponwell J, Jain P, et al., 2013. Case study of controlled air addition into landfilled municipal solid waste: Design, operation, and control. *Journal of Hazardous, Toxic, and Radioactive Waste*, 17(4): 351-359. https://doi.org/10.1061/(ASCE)HZ.2153-5515.0000183

Li LX, Fu QH, Huang JJ, 2018. Centrifuge model tests on cantilever foundation pit engineering in sand ground and silty clay ground. *Rock and Soil Mechanics*, 39(2): 529-536 (in Chinese). https://doi.org/10.16285/j.rsm.2016.0333

Li NP, Xu YS, Wang XW, 2023. Estimation of hydraulic conductivity by the modified Kozeny-Carman equation considering the derivation principle of the original equation. *Journal of Hydrology*, 621: 129658. https://doi.org/10.1016/j.jhydrol.2023.129658

Li XD, Qiu YY, Li HJ, et al., 2021. Influence of impact load on permeability of saturated calcareous sand. *Marine Georesources & Geotechnology*, 42(3): 223-232. https://doi.org/10.1080/1064119X.2023.2168577

Li YL, Tian C, Wen LF, et al., 2021. A study of the overtopping breach of a sand-gravel embankment dam using experimental models. *Engineering Failure Analysis*, 124: 105360. https://doi.org/10.1016/j.engfailanal.2021.105360

Ling H, Ling I, 2020. Centrifuge model simulations of rainfall-induced slope instability. *Journal of Geotechnical and Geoenvironmental Engineering*, 138(9): 1151-1157. https://ascelibrary.org/doi/10.1061/%28ASCE%29GT.1943-5606.0000679

Mei SY, Zhong QM, Chen SS, et al., 2022. Investigation of the overtopping-induced breach of tailings dams. *Computers and Geotechnics*, 149: 104864. https://doi.org/10.1016/j.compgeo.2022.104864

Nomura S, Yamamoto Y, Sakaguchi H, 2018. Modified expression of Kozeny-Carman equation based on semilog-sigmoid function. *Soils and Foundations*, 58(6): 1350-1357. https://doi.org/10.1016/j.sandf.2018.07.011

Ng CWW, 2014. The state-of-the-art centrifuge modeling of geotechnical problems at HKUST. *Journal of Zhejiang University-SCIENCE A (Applied Physics & Engineering)*, 15(1): 1-21. https://doi.org/10.1631/jzus.A1300217

Ng CWW, Coo JL, 2015. Hydraulic conductivity of clay mixed with nanomaterials. *Canadian Geotechnical Journal*, 52(6): 808-811. https://cdnsciencepub.com/doi/10.1139/cgj-2014-0313

Ng CWW, Farivar A, Gomaa SMMH, et al., 2021. Centrifuge modeling of cyclic nonsymmetrical thermally loaded energy pile groups in clay. *Journal of Geotechnical and Geoenvironmental Engineering*, 147(12): 04021146. https://doi.org/10.1061/(ASCE)GT.1943-5606.0002689

Qin CJ, Hazarika H, Liu GJ, et al., 2024. Seismic behavior of highway embankment reinforced with remedial countermeasures on saturated loose sandy layer. *Transportation Geotechnics*, 45: 101183. https://doi.org/10.1016/j.trgeo.2024.101183

Sailer E, Taborda DMG, Zdravkovic L, et al., 2021. Thermo-hydro-mechanical interactions in porous media: Implications on thermo-active retaining walls. *Computers and Geotechnics*, 135: 104121. https://doi.org/10.1016/j.compgeo.2021.104121

Schofield AN, 1980. Cambridge geotechnical centrifuge operations. *Geotechnique*, 30(3): 227-268. https://doi.org/10.1680/geot.1980.30.3.227

Sharma JS, Samarasekera L, 2007. Effect of centrifuge radius on hydraulic conductivity measured in a falling-head test. *Canadian Geotechnical Journal*, 44(1): 96-102. https://doi.org/10.1139/t06-092

Singh DN, Gupta KA, 2000. Modeling hydraulic conductivity in a small centrifuge. *Canadian Geotechnical Journal*, 37(1): 1150-1155. https://doi.org/10.1139/t00-027

Su LJ, Zhang YJ, Wang TX, 2014. Investigation on permeability of sands with different particle sizes. Rock and Soil Mechanics, 35(5): 1289-1294 (in Chinese). https://doi.org/10.16285/j.rsm.2014.05.034

Sun Y, Zhao Y, Zhang DL, 2019. Surface subsidence of pit-in-pit foundation in sand-obble stratum in Beijing area. *Proceedings of the Institution of Civil Engineers-Ground Improvement*, 172(2): 96-107. https://doi.org/10.1680/jgrim.17.00037

Tan TS, Scott RF, 1985. Centrifuge scaling considerations for fluid-particle systems. *Geotechnique*, 35(4): 461-470. https://doi.org/10.1680/geot.1985.35.4.461

Taylor RN, 1987. Discussion: Centrifuge scaling considerations for fluid-particle systems. *Geotechnique*, 37(1): 131-133. https://doi.org/10.1680/geot.1987.37.1.131

Thusyanthan NI, Madabhushi SPG, 2003. Scaling of seepage flow velocity in centrifuge models. CUED/D-SOILS/TR326, Cambridge University En-

Unedited

gineering Department, London, England.

Van Tonder WD, Jacobsz SW, 2017. Seepage column hydraulic conductivity tests in the geotechnical centrifuge. *Journal of the South African Institution of Civil Engineering*, 59(3): 16-24, 1525. http://dx.doi.org/10.17159/2309-8775/2017/v59n3a3

Wang LJ, Zhu B, Chen YM, et al., 2022. Centrifuge modelling on behaviour of hydrate bearing sediments during gas production by depressurization. Proceedings of the 10th International Conference on Physical Modelling in Geotechnics, p.495-499.

Wang NX, Zhang WM, Gu XW, et al., 2013. Centrifugal model test on seepage characteristics of high core rockfill dam. *Rock and Soil Mechanics*, 34(10): 2769-2773, 2780 (in Chinese).

Wang QS, Chen ZY, Sui HB, et al., 2011. Modeling seepage flow velocity in centrifuge models. *Chinese Journal of Geotechnical Engineering*, 33(8): 1235-1239 (in Chinese).

Wang Y, Ren YB, Yang Q, 2017. Experimental study on the hydraulic conductivity of calcareous sand in South China Sea. *Marine Georesources & Geotechnology*, 35(7): 1037-1047. http://dx.doi.org/10.1080/1064119X.2017.1279245

Wang Y, Shi B, Gao L, et al., 2010. Laboratory tests for temperature effects of clayey soil permeability. *Journal of Engineering Geology*, 18(3): 351-356 (in Chinese). http://dx.doi.org/10.3969/j.issn.1004-9665.2010.03.010

Wen LF, Chai JR, Wang X, et al., 2015. Behaviour of concrete-face rockfill dam on sand and gravel foundation. *Proceedings of the institution of Civil Engineers-Geotechnical Engineering*, 168(5): 439-456. http://dx.doi.org/10.1680/geng.14.00103

Xiong ZC, 2018. Analysis for heat transfer and multi-field coupling of energy geostructures. MS Thesis, Tsinghua University, Beijing, China (in Chinese).

Yang YS, Yu HT, Yuan Y, et al., 2021. 1 g Shaking table test of segmental tunnel in sand under near-fault motions. *Tunnelling and Underground Space Technology*, 115: 104080. https://doi.org/10.1016/j.tust.2021.104080

Ye W, Hu J, Ma FH, 2021. Centrifuge model study on the influence of desiccation cracks on the seepage behavior of upstream clay anti-seepage system subjected to abrupt flood. *Bulletin of Engineering Geology and the Environment*, 80: 5075-5090. https://doi.org/10.1007/s10064-021-02207-4

Ye WM, Wan M, Chen B, et al., 2013. Temperature effects on the swelling pressure and saturated hydraulic conductivity of the compacted GMZ01 bentonite. *Environmental Earth Sciences*, 68: 281-288. https://doi.org/10.1007/s12665-012-1738-4

Ye ZG, Wang LJ, Zhu B, et al., 2022. A thermo-hydro-chemo-mechanical coupled model for natural gas hydrate-bearing sediments considering gravity effect. *Journal of Natural Gas Science and Engineering*, 108: 104823. https://doi.org/10.1016/j.jngse.2022.104823

Zeng X, Su J, Wang HY, et al., 2022. Centrifuge modeling of chloride ions completely breakthrough kaolin clay liner. *Sustainability*, 14: 6976. https://doi.org/10.3390/su14126976

Zhang LC, Zhong QM, Yang M, et al., 2023. Centrifugal model tests on overtopping-induced breaching of landslide dams. *Chinese Journal of Geotechnical Engineering*, 45(s1): 197-200 (in Chinese). https://doi.org/10.11779/CJGE2023S10029

Zhao JB, Chen L, Collin F, et al., 2016. Numerical modeling of coupled thermal-hydro-mechanical behavior of GMZ bentonite in the China-Mock-up test. *Engineering Geology*, 214: 116-126. http://dx.doi.org/10.1016/j.enggeo.2016.09.015

Zhao YY, Yang Y, Ling XZ, et al., 2021. Dynamic behavior of natural sand soils and fiber reinforced soils in heavy-haul railway embankment under multistage cyclic loading. *Transportation Geotechnics*, 28: 100507. https://doi.org/10.1016/j.trgeo.2020.100507

Zheng J, Li YC, Ke H, et al., 2022. Centrifuge and numerical modeling of the impact of sediment consolidation induced by capping on contaminant transportation. *Bulletin of Engineering Geology and the Environment*, 81: 487. https://doi.org/10.1007/s10064-022-02986-4

Zhong Y, Zhou AN, Du JP, et al., 2023. Modified Kozeny-Carman equation for estimating hydraulic conductivity in nanoscale pores of clayey soils with active surfaces. *Journal of Hydrology*, 626: 130209. https://doi.org/10.1016/j.jhydrol.2023.130209

Zhu ZH, Zhang F, Dupla JC, et al., 2021. Assessment of tamping-based specimen preparation methods on static liquefaction of loose silty sand. *Soil Dynamics and Earthquake Engineering*, 143: 106592. https://doi.org/10.1016/j.soildyn.2021.106592

中文概要

题　目：离心模型试验中温度及孔隙率对砂土渗透系数的影响研究

作　者：何健健，蒋希豪，汪玉冰

机　构：浙江大学，建筑工程学院，浙江大学超重力研究中心，中国杭州，310058

目　的：离心环境下土体渗透性的准确刻画是利用离心模拟技术解决与渗流相关岩土工程问题的关键。本文旨在定性和定量研究温度、孔隙率和

离心加速度对砂土渗透特性的影响，并探讨Kozeny-Carman 方程（以下简称 KC 方程）在离心环境中的适用性，为更高试验温度、更大离心加速度下砂土渗透系数的预测提供更准确的方法。

创新点： 1. 利用自研试验装置，定性及定量揭示了温度、孔隙率及离心加速度对砂土渗透系数的影响；2. 利用本文建立的砂土渗透系数预测公式，评估了离心环境下 KC 公式的适用性。

方　法： 1. 通过自研试验装置（图 1），开展离心温控变水头渗流试验，定性揭示温度、离心加速度及孔隙率对砂土渗透系数的影响（图 7 和图 8）；2. 基于 KC 公式，通过两种拟合路径，逐步建立砂土渗透系数与温度、离心加速度和孔隙率之间的定量关系（公式(10)、公式(15)）；3. 在更高试验温度、更大离心加速度下，通过对 KC 公式及本文所建立公式的计算结果的对比，揭示 KC 公式在离心环境中的适用性（图 13）。

结　论： 1. 在相近温度及相同孔隙率下，砂土渗透系数与离心加速度呈线性相关；在相同离心加速度和相近温度下，砂土渗透系数随孔隙率函数($s^3/(1-s)^2$)几乎呈线性增加；2. 通过两种途径建立了砂土渗透系数与温度(T)、离心加速度水平(n)和孔隙率(s)之间的函数关系；3. 当离心加速度小于 50g 时，KC 方程在预测砂土渗透系数时是有效准确的，而当离心加速度超过 50g 时，利用 KC 方程预测砂土渗透系数时会存在显著误差。

关键词： 砂土渗透系数；温度；孔隙率；离心加速度；Kozeny-Carman 方程

Unedited